# Impurity-Driven Cone Formation During Laser Sputtering of Graphite

Douglas J. Krajnovich,* José E. Vázquez, Richard J. Savoy

Sputtering of highly oriented pyrolytic graphite (HOPG) by 248-nanometer laser radiation was studied. Neutral carbon atoms and small clusters were ejected with significantly higher translational energies than were expected from a simple model of thermal vaporization in the absence of a potential barrier. The HOPG also developed a remarkable surface morphology that consists of regular cones and domes. Cone formation appears to be initiated by trace metal impurities that serve as heat shunts in this highly anisotropic material.

The removal of material from the surface of a solid by high-power laser radiation (in the absence of chemicals) is often referred to as laser sputtering or laser ablation. Various mechanisms of laser sputtering have been proposed, including simple evaporation or sublimation (thermal sputtering) (*1*), melting followed by droplet emission (hydrodynamical sputtering) (*2, 3*), fracture followed by flake emission (exfoliational sputtering) (*2, 4*), and a wide range of mechanisms that involve electronic excitation effects (*4–8*). This study represents part of a broader effort to understand the energetics and mechanism of carbon sputtering and its influence on the growth and properties of carbon films. In the case of 248-nm laser sputtering of HOPG, we found that carbon atoms and small clusters were ejected with significantly higher translational energies than were predicted from a simple model (*9, 10*) of thermal vaporization in the absence of a potential barrier. We also found that HOPG develops a remarkable surface morphology consisting of regular cones and domes. Trace metal impurities that serve as heat shunts in this highly anisotropic material appear to initiate cone formation.

The HOPG material (*11*) closely approximates single-crystal graphite in which the hexagonal sheets are packed at near-theoretical density and lie parallel within a few degrees. The sample was mounted in a vacuum chamber with the basal plane exposed. Pulses of light (248 nm, 16 ns) from a KrF excimer laser were focused into a light tunnel beam homogenizer. The uniform intensity distribution at the exit face of the tunnel was re-imaged onto the sample by a fused silica lens. For the data reported here, the laser beam yielded a spot size of 2.7 mm by 3.8 mm at the sample, and the pulse energy was adjusted to give an energy fluence, $\Phi$, of 700 mJ cm$^{-2}$. Sputtered neutral carbon atoms and clusters were detected normal to the surface by an ultrahigh-vacuum mass spectrometer consisting of an electron beam ionizer, quadrupole mass filter, and particle counter. We obtained time-of-flight distributions by multiscaling the mass spectrometer signal and converting to translational energy distributions in the usual way.

The material removal rate was purposely kept low in these experiments ($\lesssim$100 Å per pulse) to avoid three-body collisions and the formation of large carbon clusters (*12*). Our goal was to study the nascent mass and translational energy distributions of the vaporizing species rather than of the condensation products. At $\Phi$ = 700 mJ cm$^{-2}$, the only neutral fragments detected are C atoms and $C_2$ and $C_3$ clusters. Although the cracking of larger clusters in the ionizer cannot be ruled out, it appears unlikely that such particles would give signals at mass-to-charge ratios of 12, 24, and 36 without showing up at some higher masses as well. The preponderance of C, $C_2$, and $C_3$ agrees with their wide presence in the equilibrium vapor over graphite at least up to 3000 K (*13*).

We measured the translational energy distribution of $C_2$ for virgin spot irradiation (Fig. 1A). The distribution appears nearly Boltzmann, but the mean translational energy of 6.4 eV is too high to reconcile with the simple thermal vaporization model discussed by Dreyfus and co-workers (*1, 9, 10*). The total sputtering yield decreases with continued irradiation, but the relative yields of C, $C_2$, and $C_3$ remain nearly constant. The falloff in sputtering yield is accompanied by a dramatic decrease in the translational energies of the fragments and a shift from Boltzmann to non-Boltzmann behavior (Fig. 1B).

The changes in sputtering dynamics correlate with the formation of an unusual surface morphology. For virgin spot irradiation, carbon removal initially proceeds in a regular layer-by-layer fashion. But within a thousand pulses, cones start to appear at apparently random locations on the surface. They appear to grow as the surrounding material is etched away at a faster rate, while new cones form in the flat areas. Eventually, the sample becomes completely covered with smooth intersecting cones (Fig. 2). This morphology is different from that produced by high-power visible laser pulses (*14*).

These changes on HOPG bear a superficial resemblance to recent results on laser ablation of polyimide (*15*). In both cases, surface morphological defects are responsible for a dramatic drop-off in etch rate and an accompanying reduction in the fragment translational energies. However, the mechanism of cone formation is entirely different in the two systems. In polyimide, this process is initiated by carbon enrichment at the sample surface. Because pure carbon has a much higher ablation threshold than the polymer, carbon enrichment increases the ablation threshold. We have referred to this effect as radiation hardening (*15*). Clearly, this phenomenon cannot occur in a single-element material, and we must look elsewhere for an explanation.

Careful examination of our laser-sputtered HOPG (Figs. 2 and 3) reveals that every cone has a small piece of foreign material at the top. Electron microprobe analysis revealed that this material consists of first-row transition metal impurities (mainly Ti, V, and Fe, although all three elements do not appear in every case). Similar-sized inclusions of the same three elements were found in HOPG samples that were reactive ion-etched in an oxygen plasma. This result proves that the metal inclusions are present in the unirradiated material (as opposed to their formation by way of

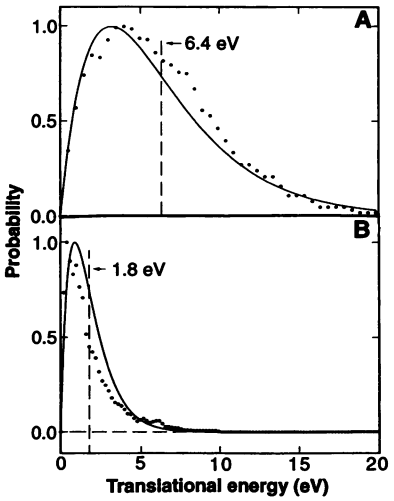


**Fig. 1.** Translational energy distributions of neutral $C_2$ molecules produced during 248-nm laser sputtering of HOPG at $\Phi$ = 700 mJ cm$^{-2}$. The sample was irradiated at an angle of incidence $\theta_{inc}$ = 45° and products were detected normal to the surface. (**A**) Irradiation of a near virgin spot and (**B**) the same spot after 2.8 × 10$^4$ laser shots. The dots represent a direct inversion of the experimental time-of-flight distributions after a small correction was made for the transit time of the $C_2^+$ ions through the mass spectrometer. The flight path from the sample to the ionizer was 69.2 cm. The curves are Boltzmann distributions with the experimental mean translational energy.

IBM Research Division, Almaden Research Center, 650 Harry Road, San Jose, CA 95120.

*To whom correspondence should be addressed.

diffusion and agglomeration reactions during laser heating). However, the shape of the inclusions is different for the two processes. After reactive ion etching (low-temperature carbon removal), the inclusions look like thin pancakes that lie parallel to the basal plane direction. After laser sputtering, the inclusions look more like irregular blobs, which suggests that the metal has melted and resolidified. The melting probably occurs when the inclusion is first exposed and the surrounding graphite is still flat and very hot. From the size and frequency of occurrence of the inclusions, we estimate that the impurity concentration (by volume) is ~50 to 100 ppm.

To determine how such tiny impurities can generate the large regular structures in Fig. 2, we must first consider details of the light absorption and heat transfer in HOPG.

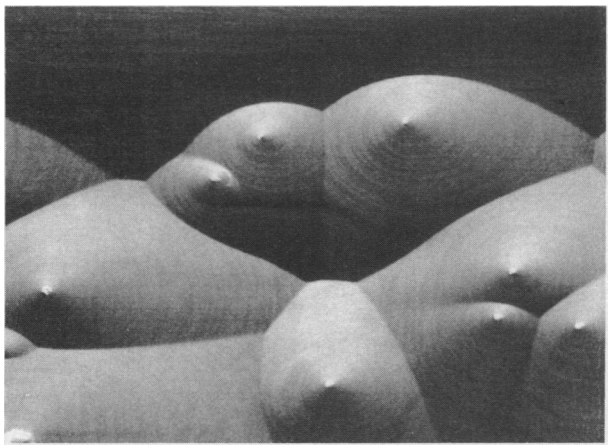

**Fig. 2.** Scanning electron microscope photograph of the same HOPG sample that was used for the data in Fig. 1. The laser beam was incident from the left at 45° to the surface normal, and the cumulative number of laser pulses was $4.3 \times 10^4$, with $\Phi = 700$ mJ cm$^{-2}$. The full width of the photograph corresponds to 0.42 mm, roughly 10% of the irradiated spot width.

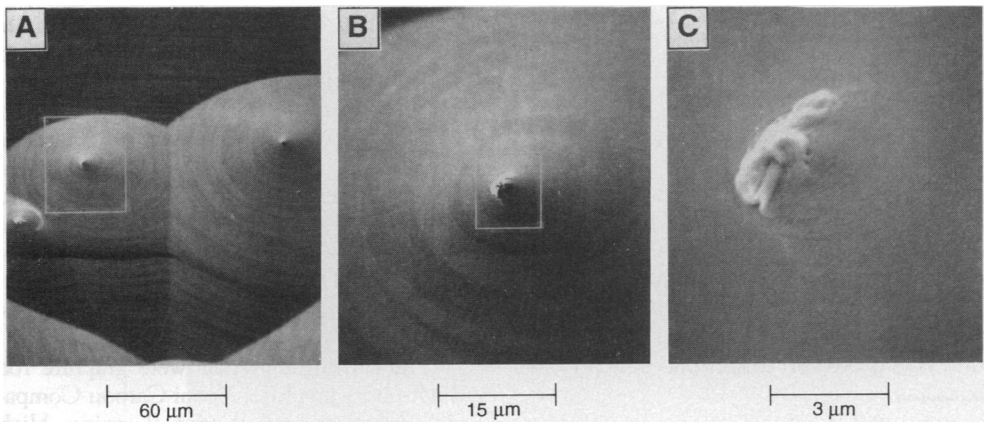


**Fig. 3.** Successively higher magnification views of an impurity-topped cone.

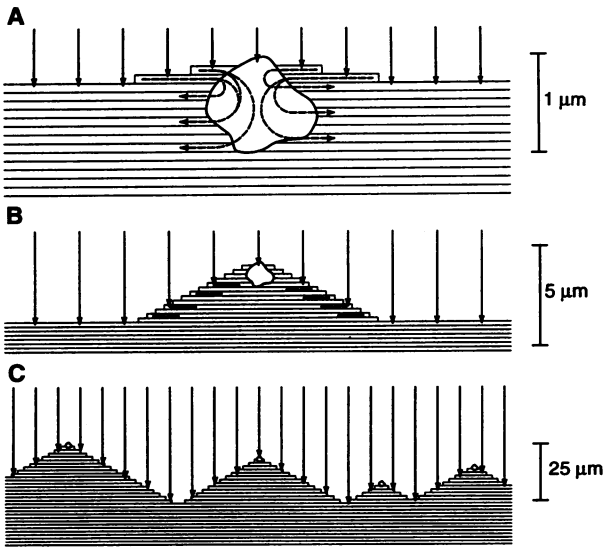


**Fig. 4.** Schematic picture of ultraviolet light absorption and heat flow. (**A**) Laser sputtering has just exposed a metal inclusion. At the scale of this drawing, each horizontal slab represents 250 carbon sheets while 99% of the (nonreflected) laser radiation is absorbed by the top 100 sheets. Heat shunting through the metal inclusion overcomes the extremely low *c*-axis thermal conductivity of graphite. (**B**) As sputtering continues, new steps form at the base of each cone where the cool staircase (with its more efficient heat sharing) meets the hot surrounding flat areas. (**C**) Sputtering virtually ceases when the entire irradiated area is covered by cones.

At 248 nm, the Beer's law absorption coefficient (*16*) of HOPG is $1.24 \times 10^6$ cm$^{-1}$, which corresponds to a 1/*e* penetration depth of 81 Å, or 24 atomic layers. The reflectivity at 248 nm is 52%, so about half of the incident light is absorbed (strictly speaking, these numbers pertain to normal incidence, but the results are similar for $\theta_{inc} = 45°$). The thermal conductivity, $k$, of HOPG is extremely anisotropic (*11*). At room temperature, the thermal conductivity parallel to the basal plane ($k_a$) is higher than that of copper, whereas that perpendicular to the basal plane ($k_c$) is ~200 times smaller. The thermal conductivity decreases at higher temperatures, but the anisotropy persists. As a result of this anisotropy, the energy absorbed from each laser pulse is initially confined to a thin layer, which brings about a high surface temperature and a high sputtering yield.

The average size of the transition metal inclusions is 1 to 3 μm. Therefore, each inclusion spans thousands of carbon sheets. The elements Ti, V, and Fe actually have lower specific heats than graphite, so that the inclusions do not make good heat sinks. Most importantly, the inclusions have isotropic thermal conductivity. Therefore, once an inclusion is exposed by sputtering, it can shunt heat efficiently from the top carbon layers to thousands of lower layers (Fig. 4A). As mentioned earlier, the shapes of the inclusions suggest that they melt and resolidify. Even if the molten transition metal reacts with carbon to form metal carbide, the inclusions will still have much higher thermal conductivities than $k_c$ of graphite. The heat shunting lowers the local surface temperature and explains why the sputtering rate slows down in the immediate vicinity of an inclusion. Once steps and terraces start to form around an inclusion, the staircase structure tends to propagate on its own because the surface temperature is lower on the staircase than in the surrounding flat areas. At any point on the staircase, laser radiation still penetrates only ~80 Å, but over any reasonably sized area the heat is clearly being shared by many more graphite sheets. On a more macroscopic scale, each radially propagating staircase represents a cone or dome (Fig. 4B). The lower temperature along the wall and at the base of each cone accounts for the decrease in mean translational energy of sputtered particles and the non-Boltzmann energy distributions. The only role of the micrometer-sized impurities is to initiate cone formation. Once initiated, each cone propagates on its own until it runs into other cones and the etching stops (Fig. 4C).

*Note added in proof*: After this work was completed, the purity of a typical HOPG sample was checked at Union Carbide by x-ray fluorescence analysis (*17*). Because the metallic impurities are inhomogeneously distributed, the HOPG sample was powdered before analysis with either sand-

paper or a jeweler's saw. The sanded powder sample showed 25 ppm Fe, 17 ppm Ti, and 14 ppm V (by weight). The saw-cut powder showed 41 ppm Fe, <5 ppm Ti, and 13 ppm V. When expressed as volume percent, these numbers become two to three times smaller. Our crude estimate of the fractional volume occupied by the metal inclusions (from the scanning electron microscope photographs) is somewhat higher, but the difference is not significant.

## REFERENCES AND NOTES


1. R. Kelly and R. W. Dreyfus, *Surf. Sci.* **198**, 263 (1988).
2. R. Kelly *et al.*, *Nucl. Instrum. Methods Phys. Res. B* **9**, 329 (1985).
3. R. Kelly and J. E. Rothenberg, *ibid.* **7/8**, 755 (1985).
4. J. E. Rothenberg and R. Kelly, *ibid.* **1**, 291 (1984).
5. R. W. Dreyfus, R. E. Walkup, R. Kelly, *Radiat. Eff.* **99**, 199 (1986).
6. R. E. Johnson and Bo U. R. Sundqvist, *Phys. Today* **45**, 28 (March 1992).
7. H. Sumi, *Surf. Sci.* **248**, 382 (1991).
8. R. Srinivasan and B. Braren, *Chem. Rev.* **89**, 1303 (1989).
9. R. W. Dreyfus, R. Kelly, R. E. Walkup, *Nucl. Instrum. Methods Phys. Res. B* **23**, 557 (1987).
10. R. W. Dreyfus *et al.*, *Proc. Soc. Photo-Opt. Instrum. Eng.* **710**, 46 (1987).
11. A. W. Moore, in *Chemistry and Physics of Carbon*, P. L. Walker, Jr., and P. A. Thrower, Eds. (Dekker, New York, 1973), vol. 11, pp. 69–187; *ibid.* (1981), vol. 17, pp. 234–286.
12. Laser vaporization sources that are used to produce large carbon clusters and fullerenes typically operate at much higher material removal rates. Often an auxiliary gas jet (or a laser-drilled channel) is used to enhance the condensation rate. See, for example, E. A. Rohlfing, D. M. Cox, A. Kaldor, *J. Chem. Phys.* **81**, 3322 (1984); A. O'Keefe, M. M. Ross, A. P. Baronavski, *Chem. Phys. Lett.* **130**, 17 (1986); W. R. Creasy, *J. Chem. Phys.* **92**, 7223 (1990).
13. P. D. Zavitsanos and G. A. Carlson, *J. Chem. Phys.* **59**, 2966 (1973); and references therein.
14. J. S. Speck, J. Steinbeck, M. S. Dresselhaus, *J. Mater. Res.* **5**, 980 (1990).
15. D. J. Krajnovich and J. E. Vázquez, *J. Appl. Phys.*, in press.
16. D. L. Greenaway, G. Harbeke, F. Bassani, E. Tosatti, *Phys. Rev.* **178**, 1340 (1969); A. Borghezi and G. Guizzeti, in *Handbook of Optical Constants of Solids II*, E. D. Palik, Ed. (Academic Press, San Diego, 1991), pp. 449–460.
17. A. W. Moore, personal communication.


18. We thank A. W. Moore of Union Carbide for providing the HOPG samples and for communicating the results of the impurity analysis and T. C. Reiley and S. A. MacDonald of IBM for help with the reactive-ion etching.

30 September 1992; accepted 15 December 1992


# Phosphorus: An Elemental Catalyst for Diamond Synthesis and Growth


Minoru Akaishi,* Hisao Kanda, Shinobu Yamaoka



**As diamond-producing catalysts, 12 transition metals such as iron, cobalt, and nickel were first reported by General Electric researchers more than 30 years ago. Since then, no additional elemental catalyst has been reported. An investigation of the catalytic action of group V elements is of great interest from the viewpoint of producing an *n*-type semiconducting diamond crystal. In the present study, diamond was synthesized from graphite in the presence of elemental phosphorus at high pressure and temperature (7.7 gigapascals and 1800°C). Furthermore, single-crystal diamond was grown on a diamond seed crystal.**


Diamond can be synthesized from graphite in the presence of any one of 12 transition metal elements (*1*, *2*), such as Fe, Ni, or Co, or in the presence of binary alloys (*3*), such as Nb-Cu alloy, carbonates (*4*), hydroxides (*5*), or sulfates (*5*, *6*) under high-pressure and high-temperature conditions in the thermodynamically stable region of diamond. The pressure and temperature conditions required for the synthesis of diamond are strongly dependent on the nature of the catalyst. For example, $CaCO_3$ does not appear to dissolve any carbon at temperatures of 1600°C (*7*), but the carbonate acts as a diamond-forming catalyst at higher temperature, above 2000°C (*3*). Some elements may therefore act as diamond-forming catalysts only at higher temperature (above 2000°C) in the thermodynamically stable region of diamond.

With respect to efforts being made to synthesize *n*-type semiconducting diamond crystal, it is very important to investigate the catalytic action of the group V elements such as P, As, Sb, and Bi in the synthesis of diamond, because these five-valent elements are considered to have donor properties in diamond. Although diamond growth experiments have been done with Sb, no diamond has been grown on a seed crystal (*8*). To the best of our knowledge, there have been no reports on the successful synthesis and growth of diamond with these five-valent elements.

Among these group V elements, P has the smallest atomic radius and is considered to be favored for accommodation in the small diamond lattice. We were able to synthesize diamond in the presence of elemental P under comparatively high pressure and temperature conditions (6.5 to 7.7 GPa and 1800° to 2200°C). Furthermore, diamond single crystal was successfully grown on a natural single-crystal diamond at a lower pressure and temperature (6.5 GPa and 1750° to 1800°C) in the presence of elemental P.

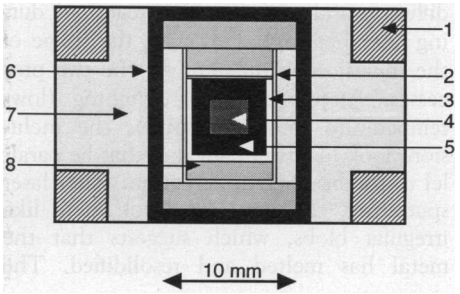


**Fig. 1.** Sample assembly for the high-pressure synthesis of diamond using a P catalyst: 1, steel ring; 2, Mo foil; 3, Mo capsule; 4, red P; 5, graphite capsule; 6, graphite heater; 7, NaCl–10% $ZrO_2$ by weight pressure medium; 8, NaCl–20% $ZrO_2$ by weight pressure medium.

Synthesis experiments were carried out with a modified belt type high-pressure apparatus with a bore diameter of 32 mm (*9*). Pressure was calibrated at room temperature by means of the known pressure-induced phase transitions of Bi, Tl, and Ba. Temperature was estimated from the extrapolated relations between the input power and the temperature, which we had obtained in advance by measuring the temperature up to 1800° and 2100°C with Pt6%Rh-Pt30%Rh and W5%Re-W26%Re thermocouples, respectively. The pressure effect on the electromotive force of the thermocouple was not corrected.

The starting materials were graphite rod (high-purity graphite, Tokai Carbon Company) and elemental P (red P grains, High Purity Company; stated purity, 99.9999%). The P was pulverized with an agate mortar, and the powder was dried at 110°C in an oven before use. The graphite rod was machined into the desired shape as shown in Fig. 1. The P powder was put into a capsule made of graphite and loaded in a capsule made of Mo at 200 MPa. The encapsulated sample was then placed in an outer Mo capsule made of Mo foil. The sample was maintained at 7.7 GPa and 2200°C for 10 min.

The product that we obtained was tightly covered with Mo, which was removed with a nipper. The recovered sample was examined with an optical microscope and an x-ray diffractometer. Diamond was formed and no graphite was detected in the sample according to the x-ray diffraction patterns, which were the same as those of natural or synthetic samples. Many tiny crystals were observed around the P with an optical microscope. This result suggests that the graphite capsule


National Institute for Research in Inorganic Materials, 1-1 Namiki, Tsukuba-shi, Ibaraki, 305, Japan.

*To whom correspondence should be addressed.